condensed matter

MDPI

Article

Reflection Efficiency and Spectra Resolutions Ray-Tracing Simulations for the VOXES HAPG Crystal Based Von Hamos Spectrometer

Veronica De Leo [1,*], Alessandro Scordo [2], Catalina Curceanu [2], Marco Miliucci [2,*] and Florin Sirghi [2]

[1] Dipartimento di Fisica, Università degli Studi di Roma "La Sapienza", Sezione INFN Roma 1, P.le Aldo Moro 5, 00185 Rome, Italy

[2] Laboratori Nazionali di Frascati, Via E. Fermi 54, 00044 Frascati, Italy; alessandro.scordo@lnf.infn.it (A.S.); catalina.curceanu@lnf.infn.it (C.C.); fsirghi@lnf.infn.it (F.S.)

* Correspondence: vdeleo@roma1.infn.it (V.D.L.); Marco.Miliucci@lnf.infn.it (M.M.)

Abstract: The VOXES collaboration at INFN National Laboratories of Frascati developed a prototype of a high resolution Von Hamos X-ray spectrometer using HAPG (Highly Annealed Pyrolytic Graphite) mosaic crystals. This technology allows the employment of extended isotropic sources and could find application in several physics fields. The capability of the spectrometer to reach energy precision and resolution below 1 and 10 eV, respectively, when used with wide sources, has been already demonstrated. Recently, the response of this device, for a ρ = 206.7 mm cylindrically bent HAPG crystal using $CuK\alpha_{1,2}$ and $FeK\alpha_{1,2}$ XRF lines, has been investigated in terms of reflection efficiency by a dedicated ray-tracing simulation. Details of the simulation procedure and the comparison with the experimental results are presented. This study is crucial in order to retrieve information on the spectrometer signal collection efficiency, especially in the energy range in which the standard calibration procedures cannot be applied.

Keywords: Von Hamos spectrometer; HAPG crystal; ray-tracing simulation; reflection efficiency

Citation: De Leo, V.; Scordo, A.; Curceanu, C.; Miliucci, M.; Sirghi, F. Reflection Efficiency and Spectra Resolutions Ray-Tracing Simulations for the VOXES HAPG Crystal Based Von Hamos Spectrometer. *Condens. Matter* **2022**, *7*, 1. https://doi.org/10.3390/condmat7010001

Academic Editor: Amir-Abbas Haghighirad

Received: 29 October 2021
Accepted: 20 December 2021
Published: 24 December 2021

1. Introduction

One of the most quoted methods to perform high energy resolution X-ray measurements both in laboratory experiment and synchrotron radiation facility is provided by the Bragg spectroscopy. The requirement on the size of the target not to exceed tens of microns represents the major hindrance in its use when photons emitted from extended sources (millimetric) need to be measured [1]. In addition, the typical very low efficiencies of Bragg spectrometers prevent them from being used in several applications. The prototype of a high resolution Von Hamos X-ray spectrometer using HAPG (Highly Annealed Pyrolytic Graphite) mosaic crystals developed by the VOXES collaboration at INFN National Laboratories of Frascati offers the possibility to achieve few eV energy resolution for energies going from 2 keV up to 10 of keV and to measure not only collimated sources, but also extended ones. Highly Annealed Pyrolitic Graphite (HAPG) is a mosaic crystal consisting in a large number of nearly perfect small crystallites. The crystallites distribution can be described by a Gaussian function and the mosaicity is defined as the FWHM of this distribution. It makes it possible that a photon can find a crystallite plane at the right Bragg angle and be reflected unless if it is slightly deviated from reaching the crystal with the exact Bragg relation [2,3]. This property together with a lattice spacing constant $d = 3.514$ Å, enables them to be highly efficient in the 2–20 keV energy range. The peak reflectivity is always lower than one and depends on the diffraction volume and on the crystal thickness. It is equal to unity for perfect crystals only. The mosaic crystals technology is suitable to be used in the Von Hamos configuration combining the standard dispersion of a flat crystal with the focusing properties of cylindrically bent crystals.

Several studies aimed to analyze the effect on the energy resolution of the precision of the mosaicity and thickness of the crystal have been already performed, and the capability

of the spectrometer to be optimized in order to achieve the best precision has been also demonstrated [4,5].

The performance of the spectrometer has been lately studied in terms of reflection efficiency [6] and in this work we want to focus on the ray-tracing simulations implemented in order to check the agreement with the experimental results. The achievement of consistent results is fundamental to evaluate the efficiency of the spectrometer. In the next sections the description of the experimental setup and procedure, of the ray-tracing simulations, and the comparison of the experimental and simulated data are presented.

2. Setup

In the spectrometer configuration used in our measurements the X-ray source and the position detector are placed on the axis of a cylindrical crystal. This configuration is known as Von Hamos and allows to increase the reflection efficiency due to the vertical focusing. This geometry permits to determine the source-crystal and the source-detector distances, L_1 and L_2, respectively, by means of the Bragg angle (θ_B) and of the curvature radius of the crystal (ρ_c):

$$L_1 = \frac{\rho_c}{sin_{\theta_B}} \quad (1)$$

$$L_2 = 2\, L_1\, sin\phi \quad (2)$$

where $\phi = \pi - \theta_B$.

Adding a pair of slits to this configuration, it is possible to shape the beam of the X-rays emitted by an extended target modifying the position (Z_1 and Z_2) and the apertures (S_1 and S_2) of the slits to create a virtual point-like source (Z_f), an angular acceptance $\Delta\theta'$ and an effective source S'_0 (see Figure 1 for the horizontal plane of the beam) [5].

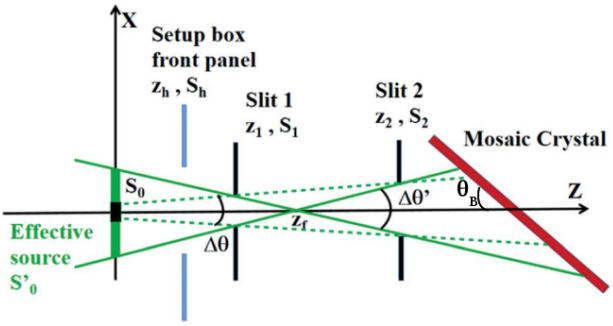

Figure 1. XRF beam dispersive plane (not in scale) where is represented the slits system (S_1 and S_2), the virtual and effective sources, S_0 and S'_0, the angular acceptance $\Delta\theta'$, the Bragg angle θ_B and the mosaic crystal (see [5] for more details).

The experimental apparatus consists of a XTF-5011 Tungsten anode X-ray tube produced by OXFORD INSTRUMENTS, located on the top of an aluminum box where a 125 μm thick target foil is contained. The center of the foil is the source position and it is placed on a 45° target holder.

The two adjustable motorized slits (STANDA 10AOS10-1) with 1 mm sensitivity are arranged after the circular exit window of the aluminum box of 5.9 mm diameter. The HAPG crystal used for the measurements has a thickness of 100 μm, a curvature radius (ρ_c) of 206.7 mm and mosaicity (ω) of 0.1°. The position detector, also equipped with a positioning motorized system, is a commercial MYTHEN2-R-1D 640 channels strip detector produced by DECTRIS (Zurich, Switzerland). The active area is 32 × 8 mm^2; strip width and thickness are, respectively, 50 μm and 420 μm; further details can be found in [5].

3. Experimental Procedure

The spectrometer setup was optimized for the measurement of the two Cu and Fe $K\alpha$ lines. The target foil is activated by the X-ray tube and the $K\alpha_{1,2}$ lines, isotropically

emitted, are collimated by the slits system to simulate a point-like source. An example of the resulting spectrum, after performing the calibration and fitting procedure reported in our previous work [5], is shown in the Figure 2. In this case the slits are set to maintain an angular divergence $\Delta\theta$ of 0.7° and the distances between the source-to-HAPG crystal and crystal-to-detector are of 900.54 mm. The alignment of the optical system has been performed by using a laser.

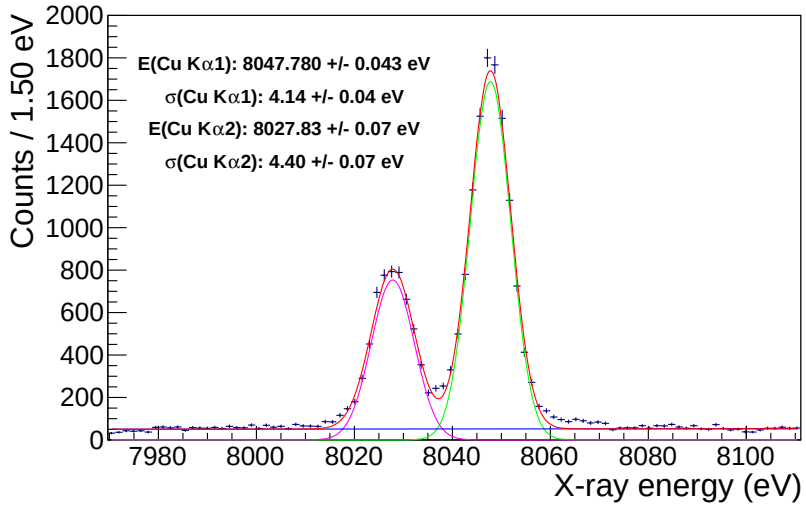

Figure 2. Copper Bragg spectrum where the overall fitting function (red), the polynomial background (blue) and the $K\alpha_1$ (green) and $K\alpha_2$ (violet) components are over imposed to the spectrum for $\Delta\theta$ = 0.7 and S'_0 = 1.1 mm, elaborated from [5] (see text for details).

These kind of spectra are used in the evaluation of the HAPG crystal reflection efficiency. Usually this quantity is defined as the percentage of Bragg reflected X-rays of a given energy E_0 for different impinging angles and is obtained from X-ray beam emitted from a monochromatic point-like source. Instead, the quantity we want to measure is the following:

$$\epsilon^R_{\Delta\theta',S'_0} = \frac{R^r_{\Delta\theta',S'_0}}{R^i_{\Delta\theta',S'_0}} \tag{3}$$

It represents the ratio between the number of $Cu(K_{\alpha 1,2})$ or $Fe(K_{\alpha 1,2})$ X-rays reflected from the crystal ($R^r_{\Delta\theta',S'_0}$) and that of those impinging on it ($R^i_{\Delta\theta',S'_0}$) for different source sizes S'_0 and beam divergence $\Delta\theta'$ pairs [6]. The numerator of Equation (3) is obtained from the Bragg energy spectrum $R^B_{\Delta\theta',S'_0}$, as the one shown in Figure 2, taking into account the X-ray transmission in air (T_{air}) and the MYTHEN2 detection efficiency (QE^M):

$$R^r_{\Delta\theta',S'_0} = R^B_{\Delta\theta',S'_0} \frac{1}{T_{air}} \frac{1}{QE^M} \tag{4}$$

The T_{air} coefficient is evaluated, for a given energy and HAPG-MYTHEN2 distance, from the CXRO database [7] while QE^M is provided by the producers. In the Figure 3 and the resulting behaviour of the transmission coefficient with the energy is shown; the fit carried out in the energy range of interest for our measurements is represented in red.

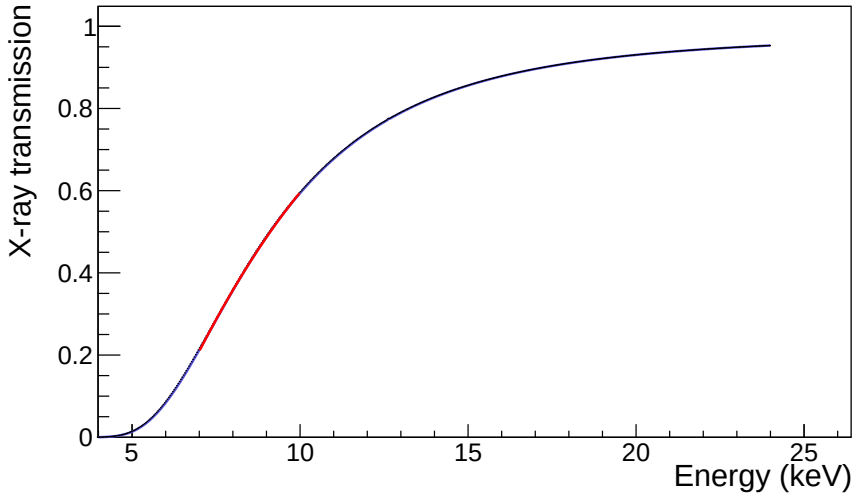

Figure 3. The X-ray transmission coefficient in air at 90.05 cm function of energy; the performed fit in the energy range of our interest is represented in red.

The determination of the number of X-rays impinging on the crystal ($R^{i}_{\Delta\theta',S'_0}$) required a longer procedure. First of all, for each $S'_0\,\Delta\theta'$ combination, a measurement with the MYTHEN2 detector in place of the HAPG crystal has been performed in order to quantify the X-rays reaching the HAPG position that we defined as MYTHEN2 direct measurements $R^{M}_{\Delta\theta',S'_0}$. However, since with the MYTHEN2 detector we can set only an energy threshold and we have to find the numbers of pure $Cu(K_{\alpha 1,2})$ or $Fe(K_{\alpha 1,2})$ signal, we needed of the help of a Silicon PinDiode to extract the ratio $R(S/B)$ between the $Cu(K_{\alpha 1,2})$ or $Fe(K_{\alpha 1,2})$ lines and all the other background photons, produced by Bremmstrahlung or other processes occurring in the source box and reaching the crystal, having also exceeded the set energy threshold. The spectrum is bin by bin corrected accounting for the different efficiencies of the PinDiode and of the MYTHEN2 detector (see Figure 4):

$$Bin_{PD_{corr}} = Bin_{PD} \times QE^{M}/QE^{PD} \tag{5}$$

The number of X-rays impinging on the HAPG crystal can then be evaluated from the following relation:

$$R^{i}_{\Delta\theta',S'_0} = R^{M}_{\Delta\theta',S'_0}\frac{1}{QE^{M}}R(S/B)\frac{A_c}{8\text{ mm}} \tag{6}$$

where the ratio between the beam vertical dimension A_c and 8 mm accounts for the difference between the MTYTHEN2 strip height and the XRF beam spot vertical size on the HAPG. A_c is evaluated, following the procedure described in [5], from the slits positions and dimensions.

The reflection efficiencies, obtained with a $\rho = 206.7$ mm HAPG crystal for both $Cu_{K\alpha 1,2}$ $Fe_{K\alpha 1,2}$ XRF lines, from Equations (4) and (6), are estimated as [6]:

$$\epsilon^{R}_{\Delta\theta',S'_0} = \frac{8R^{B}_{\Delta\theta',S'_0}}{T_{air}R^{M}_{\Delta\theta',S'_0}R(S/B)A_c} \tag{7}$$

and resulted to vary between 0.15–0.35 and 0.1–0.3 for copper and iron, respectively.

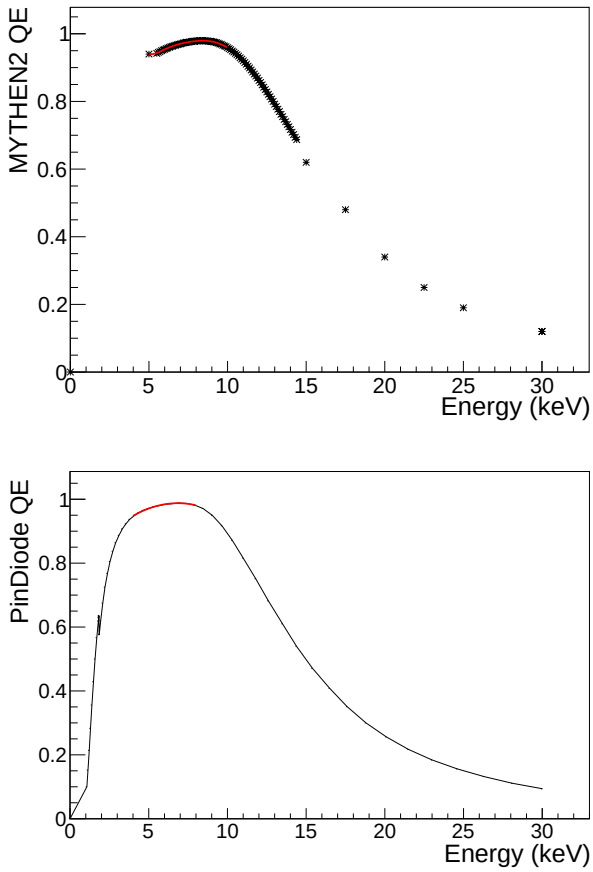

Figure 4. MYTHEN2 detector (**top**) and PinDiode quantum efficiencies (**bottom**) as a function of energy provided by the producers; the performed fit in the energy range of our interest is represented in red.

4. Ray-Tracing Simulations

In this section we present the comparison of the performances of the VOXES spectrometer with the ones obtained from the ray-tracing simulations. We used the XOP+SHADOW3 software [8–10] implemented in the Oasys enviroment [11]. The XOP package includes all the codes that are necessary to evaluate the interaction of the X-rays with the optical components defined by the user. In particular, we choose an extension, the *SHADOWVUI* package that provides a Visual User Interface for the SHADOW ray-tracing program. The elements of the optical system are defined by objects that are called *widgets* within a canvas that represents our workspace. Each widget contains the user-defined parameters by double-clicking on it and has to be connected with others by connectors. The *Loop Point* widget allows to increase the statistics performing several runs of smaller size and can be used also to start the simulation from the source widget which we refer to as *target*.

The *target* is generated by means of Shadow Geometrical Source and we defined it as a 12×1.3 mm rectangular 0.1 mm thick to prevent any losses. In the same widget we provide as input the energy spectrum of the copper (or iron) X-rays. It is sampled with a double Lorentzian function, the widths of which are obtained from the paper [12]. In the snapshot of the Figure 5 from the Geometrical Source widget, an example of the copper spectrum input is reported; on the left we inserted the energy range of the spectrum, the binning and the path of the input file while on the right the histogram statistics is listed. After that, we defined other two widgets that include two python codes to take into account the target rotation of 45° and to consider the X-ray divergence.

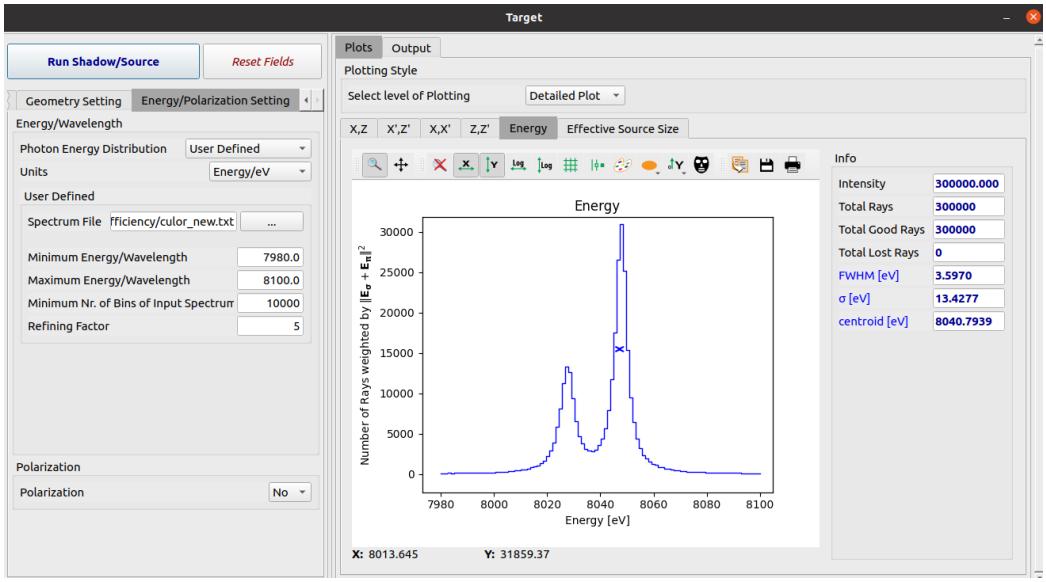

Figure 5. Snapshot of the *target* widget where the energy spectrum given in input to the simulation is visible.

Then, we implement the description of the box hole and the two slits system in order to be able to set their positions and apertures. These last two widgets have a very important role in the simulation because they define the effective source size S_0' and the angular divergence $\Delta\theta'$. The snapshot of the Figure 6 is referred to the widget of the first slit used in the simulation of the copper Bragg spectra for $\Delta\theta' = 0.7°$ and $S_0' = 1.1$ mm; in the right part the setting of the position are shown while on the center, the two-dimensional XZ plot, together with the corresponding projections of the beam dimensions, are reported. In these plots, it is possible to notice the effective source size of 1.1 mm. The following step consists in the simulation of the HAPG crystal by using the Shadow Spherical Crystal widget. Here, we defined the geometry of the crystal, using the cylindrical one, and we introduced the value of the curvature radius ($\rho_c = 206$ mm), the mosaicity ($\omega = 0.1°$), usually provided by the producer, the position and the nominal Bragg angle at which the reflection occurs as shown in the snapshot reported in the Figure 7 on the left column; on the center instead, the XZ plot of the XRF photons emitted from the effective source and reflected by the HAPG crystal is shown in case of a copper target $\Delta\theta' = 0.7°$ and $S_0' = 1.1$ mm, together with the projections, in arbitrary units, of the Z and X coordinates on the right and on the bottom of the two-dimensional plot respectively. The Z-plot converted in energy and fitted with a Gaussian function is shown in the Figure 8 where it is possible to appreciate the good matching of the two XRF emission lines $K\alpha_{1,2}$ both in terms of energy and resolution with the experimental one of the Figure 2. The small difference between the resolution values is attributable to small deviation, at micrometer level, of the position and/or aperture of the slits from the nominal ones.

To evaluate the reflection efficiencies from the simulations we used the following ratio [6]:

$$\epsilon^{R,Sim}_{\Delta\theta',S_0'} = \frac{Intensity_{\Delta\theta',S_0'}}{Good\ rays_{\Delta\theta',S_0'}} \tag{8}$$

where $Good\ rays_{\Delta\theta',S_0'}$ refers to the number of photons emitted by the source and reaching the MYTHEN2 detector, while $Intensity_{\Delta\theta',S_0'}$ accounts also for the HAPG crystal reflectivity. These quantities are displayed in the right part of the snapshot of the Figure 7.

The results obtained in terms of reflection efficiency for different effective source sizes, S_0', as a function of the angular divergence $\Delta\theta'$ from simulated data are shown for copper and iron in Figures 9 and 10, respectively, in the top pads, while the differences between the experimental and the simulated efficiency are given in the bottom pads.

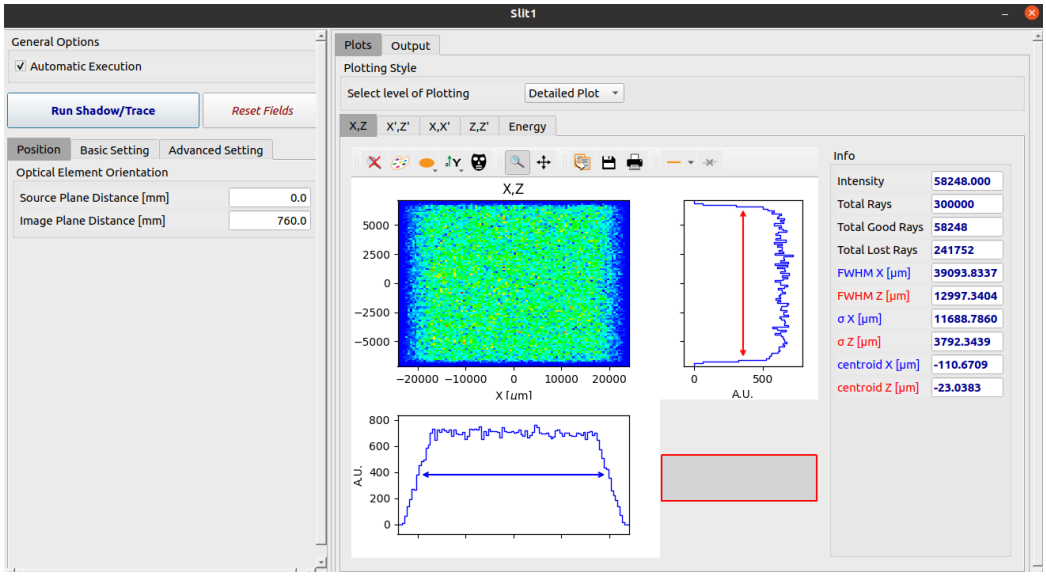

Figure 6. Snapshot of the slit widget used in the simulation of the copper Bragg spectra for $\Delta\theta' = 0.7°$ and $S_0' = 1.1$ mm; in the right part the setting of the position is shown while on the center, the two-dimensional XZ plot, together with the corresponding projections of the beam dimensions are visible.

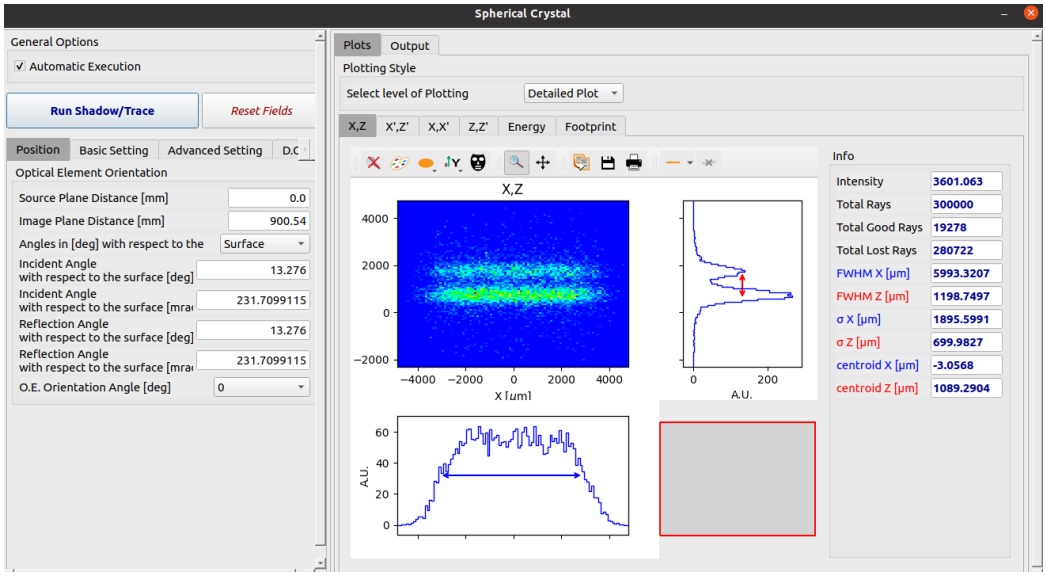

Figure 7. XZ plot of the XRF photons, emitted from the effective source and reflected by the HAPG crystal, as seen from the MYTHEN2 detector point of view (top); intensity as a function of the Z-coordinate (bottom).

The results highlight how the simulation well reproduces the experimental data within the associated errors. For each point of the simulated reflection efficiencies plots, the error bars are the result of the sum in quadrature of the statistical (almost negligible) and systematic errors. To evaluate the systematic uncertainty we performed simulations fixing the S_0' and $\Delta\theta'$ values and varying different parameters as the position of the slits, crystal and MYTHEN detector (± 5 mm), the opening of the slits (± 0.05 mm), their possible misalignment in the x-coordinate (± 5 mm) and in the z-coordinate (± 0.1 mm), and finally the mosaicity ($\pm 0.01°$).

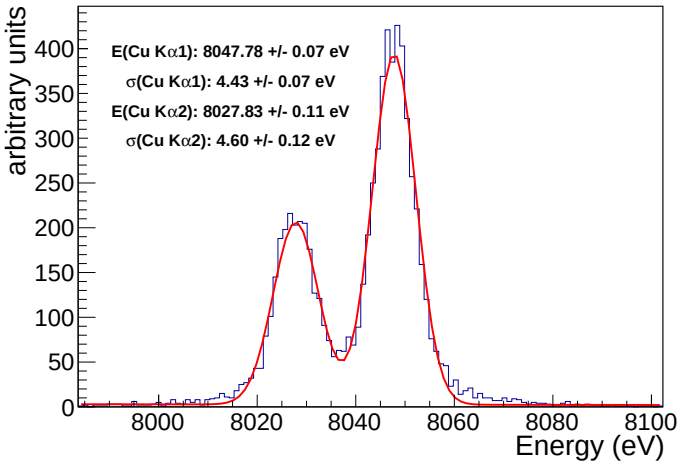

Figure 8. Simulated spectrum after energy conversion and fit with a gaussian function for copper, $\Delta\theta' = 0.7$, $S'_0 = 1100$ mm.

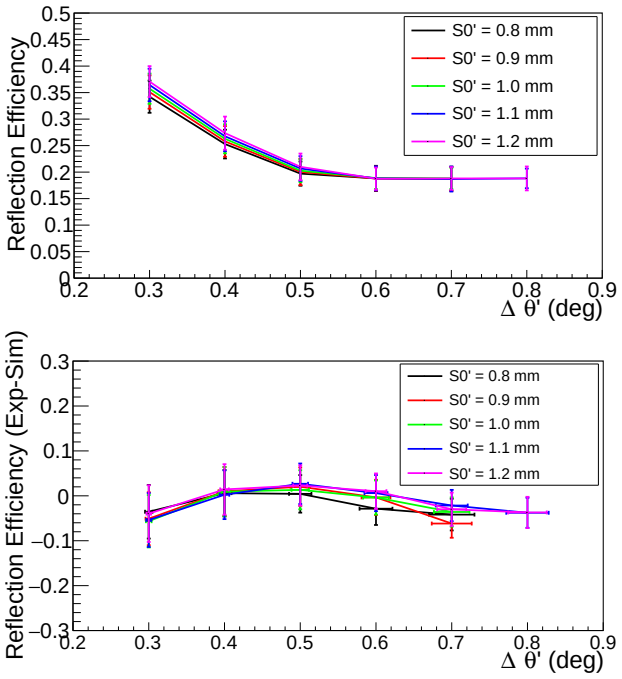

Figure 9. Reflection efficiency from simulations (**top**) and difference between the experimental and simulated reflection efficiency (**bottom**) for copper, ($\rho = 206$ mm) [6].

The consequent variation of the reflection efficiency values has been accounted as systematic error. In the Figure 11 we reported the study carried out in case of use of a copper target for $\Delta\theta' = 0.7°$, $S'_0 = 1.1$ mm. Since the expected uncertainty on the mosaicity value of the used HAPG crystal is at the level of 0.01°, we performed the systematics analysis studying its variation between 0.09° and 0.11°. In particular, on top the reflection efficiencies obtained for mosaicity values 0.09°, 0.10° and 0.11° are represented in blue, cyan and magenta, respectively, while on bottom the systematic uncertainties referred to all analyzed parameters are summarized. As one can see, most parameters gave a contribution less than 5 per mill while the variation of the mosaicity resulted of the order of 2%. This value has been taken as systematic uncertainty associated to the reflection efficiency.

The number of events used as input in the simulations has been chosen according to the plot shown in Figure 12, where the statistical error on the reflection efficiency ($\delta\epsilon_{stat}$) as a function of the MC simulated events, as example, for the $S'_0 = 1100$ µm, and $\Delta\theta' = 0.7°$ copper case, is reported. In our final simulations, we used 1.5×10^6 events not to affect the precision of the efficiency simulations by low statistics.

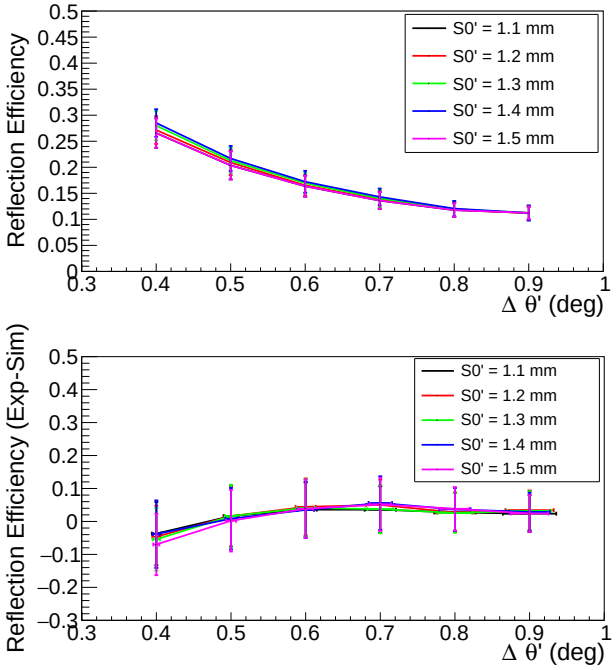

Figure 10. Simulated reflection efficiency (**top**) and difference between the experimental and simulated reflection efficiency (**bottom**) for iron, (ρ = 206 mm) [6].

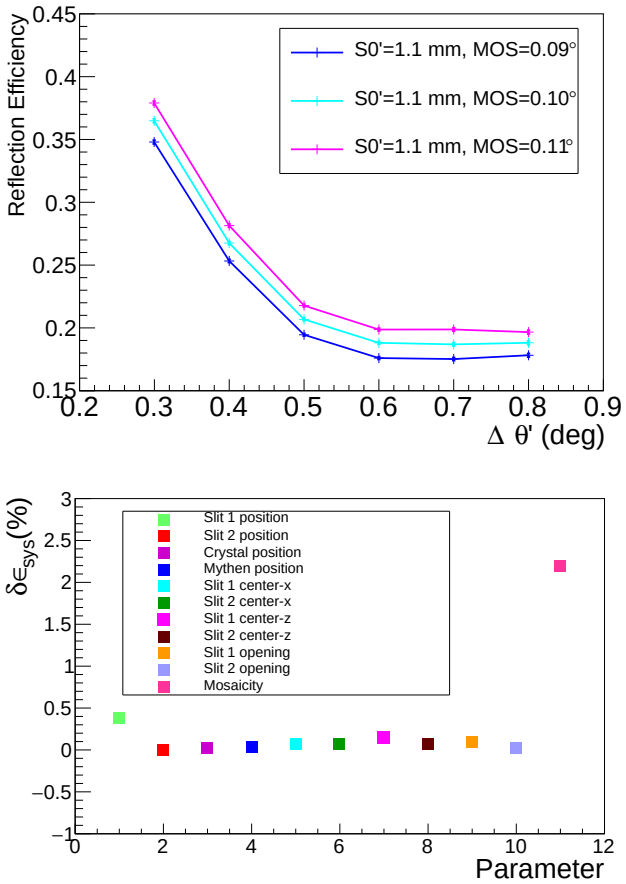

Figure 11. Reflection efficiencies obtained for mosaicity values 0.09°, 0.10° and 0.11° are represented in blue, cyan and magenta, respectively (**top**). Contributions to the systematic uncertainties for copper $S_0' = 1100$ µm and $\Delta\theta' = 0.7°$ (**bottom**).

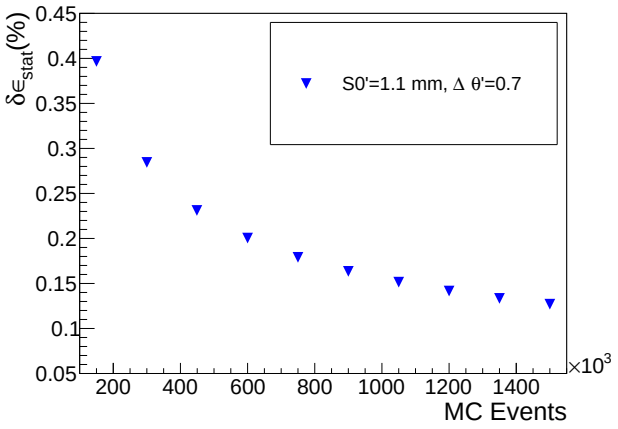

Figure 12. Variation of the statistical error on the reflection efficiency as a function of the number of generated events.

5. Discussion

In this work we presented the experimental procedure followed to carry out the reflection efficiency measurements for ρ = 206.7 mm cylindrically bent HAPG crystal using $CuK\alpha_{1,2}$ and $FeK\alpha_{1,2}$ XRF lines. The results highlight that the measured reflection efficiencies appear almost unaffected by the source size while show a slight dependence on the beam divergence.

The simulation software and each step of the simulations performed in order to check the consistency with the experimental data were also described. The response of the spectrometer has been validated by the ray tracing simulations, both in terms of the spectra reproduction and of the reflection efficiency measurement and a good agreement within the errors was found. Consistent and reliable simulated data are crucial to get information on the efficiency of the spectrometer which is fundamental for the experimental apparatus for the proposal of future experiments.

Author Contributions: Conceptualization, A.S.; methodology, A.S.; software, V.D.L.; validation, A.S. and V.D.L.; formal analysis, A.S.; investigation, A.S., V.D.L. and M.M.; resources, A.S., M.M. and F.S.; data curation, A.S., V.D.L. and M.M.; writing—original draft preparation, V.D.L.; writing—review and editing, V.D.L.; visualization, V.D.L; supervision, A.S. and C.C.; project administration, A.S.; funding acquisition, A.S. All authors have read and agreed to the published version of the manuscript.

Funding: This work was supported by the 5th National Scientific Committee of INFN in the framework of the Young Researcher Grant 2015, n. 17367/2015. This project has received funding from the European Union's Horizon 2020 research and innovation program EU STRONG-2020, under grant agreement No 824093.

Acknowledgments: We thank the LNF and SMI staff, in particular the LNF SPCM service and Doris Pristauz-Telsnigg, for the support in the preparation of the setup. Figures 1, 2, 9 and 10 are reproduced from Refs. [5,6] with permission from the Royal Society of Chemistry.

Conflicts of Interest: The authors declare no conflict of interest.

References

1. Barnsley, R.; Peacock, N.J.; Dunn, J.; Melnick, I.M.; Coffey, I.H.; Rainnie, J.A.; Tarbutt, M.R.; Nelms, N. Versatile high resolution crystal spectrometer with X-ray charge coupled device detector. *Rev. Sci. Instrum.* **2003**, *74*, 2388. [CrossRef]
2. Legall, H.; Stiel, H.; Antonov, A.; Grigorieva, I.; Arkadiev, V.; Bjeoumikhov, A. A new generation of X-ray optics based on pyrolitic graphite. In Proceedings of the FEL 2006, Berlin, Germany, 27 August–1 September 2006; BESSY: Berlin, Germany, 2006; p. 798.
3. Grigorieva, I.G.; Antonov, A.A. HOPG as powerful X-ray optics. *X-ray Spectrom.* **2003** *32*, 64–68. [CrossRef]
4. Scordo, A.; Curceanu, C.; Miliucci, M.; Sirghi, F.; Zmeskal, J. Pyrolitic Graphite Mosaic Crystal Thickness and Mosaicity Optimization for an Extended Source Von Hamos X-ray Spectrometer. *Condens. Matter* **2019**, *4*, 38. [CrossRef]

5. Scordo, A.; Breschi, L.; Curceanu, C.; Miliucci, M.; Sirghi, F.; Zmeskal, J. High resolution multielement XRF spectroscopy of extended and diffused sources with a graphite mosaic crystal based Von Hamos spectrometer. *J. Anal. At. Spectrom.* **2020**, *35*, 155–168. [CrossRef]
6. Scordo, A.; De Leo, V.; Curceanu, C.; Miliucci, M.; Sirghi, F. Efficiency measurements and simulations of a HAPG based Von Hamos spectrometer for large sources. *J. Anal. At. Spectrom.* **2021**, *36*, 2485–2491. [CrossRef]
7. Henke, B.; Gullikson, E.; Davis, J. X-ray interactions: Photoabsorptions, scattering, transmission, and reflection at E = 50–30,000 eV, Z = 1–92. *Atomic Data Nucl. Data Tables* **1993**, *54*, 181–342. [CrossRef]
8. Sanchez del Rio, M.S.M.; Bernstorff, S.; Savoia, A.; Cerrina, F. A conceptual model for ray tracing calculations with mosaic crystals. *Rev. Sci. Instrum.* **1992**, *63*, 932–935. [CrossRef]
9. Sanchez del Rio, M.S.M.; Canestrari, N.; Jiang, F.; Cerrina, F. SHADOW3: A new version of the synchrotron X-ray optics modelling package. *J. Synchrotron Radiat.* **2011**, *18*, 708–716. [CrossRef] [PubMed]
10. Rebuffi, L.; del Rio, M.S. ShadowOui: A new visual environment for X-rayoptics and synchrotron beamline simulations. *J. Synchrotron Radiat.* **2016**, *23*, 1357–1367. [CrossRef] [PubMed]
11. Rebuffi, L.; del Rio, M.S. OASYS (OrAnge SYnchrotron Suite): An open-source graphical environment for X-ray virtual experiments. *Int. Soc. Opt. Photonics* **2017**, *10388*, 103880S.
12. Ménesguen, Y.; Lepy, M.C.; Hönicke, P.; Müller, M.; Unterumsberger, R.; Beckhoff, B.; Hoszowska, J.; Dousse, J.C.; Błachucki, W.; Ito, Y.; et al. $K\alpha_{1,2}$ and $K\beta_{1,3}$ X-ray emission lines of the 3d transition metals. *Phys. Rev. A* **1997**, *56*, 4554–4568.